A novel Rac1 GAP splice variant relays poly-Ub accumulation signals to mediate Rac1 inactivation

Timothy Y. Huang[a], Sarah Michael[b], Tao Xu[c], Ali Sarkeshik[c], James J. Moresco[c], John R. Yates, III[c], Eliezer Masliah[b], Gary M. Bokoch[a], and Céline DerMardirossian[a]

[a]Department of Immunobiology and Microbial Science and [c]Department of Chemical Physiology, Scripps Research Institute, La Jolla, CA 92037; [b]Department of Experimental Neuropathology, University of California, San Diego, La Jolla, CA 92093

ABSTRACT **Spatial control of RhoGTPase-inactivating GAP components remains largely enigmatic. We describe a brain-specific RhoGAP splice variant, BARGIN (BGIN), which comprises a combination of BAR, GAP, and partial CIN phosphatase domains spliced from adjacent SH3BP1 and CIN gene loci. Excision of BGIN exon 2 results in recoding of a 42–amino acid N-terminal stretch. The partial CIN domain is a poly-ubiquitin (poly-Ub)–binding module that facilitates BGIN distribution to membranous and detergent-insoluble fractions. Poly-Ub/BGIN interactions support BGIN-mediated inactivation of a membranous Rac1 population, which consequently inactivates membrane-localized Rac1 effector systems such as reactive oxygen species (ROS) generation by the Nox1 complex. Given that Ub aggregate pathology and proteotoxicity are central themes in various neurodegenerative disorders, we investigated whether BGIN/Rac1 signaling could be involved in neurodegenerative proteotoxicity. BGIN/Ub interactions are observed through colocalization in tangle aggregates in the Alzheimer's disease (AD) brain. Moreover, enhanced BGIN membrane distribution correlates with reduced Rac1 activity in AD brain tissue. Finally, BGIN contributes to Rac1 inhibition and ROS generation in an amyloid precursor protein (APP) proteotoxicity model. These results suggest that BGIN/poly-Ub interactions enhance BGIN membrane distribution and relay poly-Ub signals to enact Rac1 inactivation, and attenuation of Rac1 signaling is partially dependent on BGIN in a proteotoxic APP context.**

Monitoring Editor
Josephine C. Adams
University of Bristol

Received: Aug 1, 2012
Revised: Nov 5, 2012
Accepted: Nov 26, 2012

INTRODUCTION

The spatial regulation of RhoGTPase activity is complex and requires the coordinated activity of exchange factors, GTPase-activating components (GAPs), and RhoGDI (Jaffe and Hall, 2005). Binary switching of the RhoGTPases between GTP-loaded active and GDP-bound inactive states is further complicated by the immense redundancy in the regulatory components that activate and inactivate RhoGTPases. More specifically, RhoGAPs comprising a signature GAP domain are massively overrepresented in relation to their target substrates, with >50 GAP signaling components encoded in the human genome (Tcherkezian and Lamarche-Vane, 2007). This raises the question as to why such redundancy exists for the inactivation of Rho-family GTPases.

The BAR-domain RhoGAP subfamily (hereby referred to as the BAR-RhoGAP subfamily) comprises four family members described so far (oligophrenin, RICH1, RICH2, SH3BP1) that all share an identical domain architecture with an N-terminal, lipid curvature–sensing BAR domain, an intermediary RhoGAP module, and a C-terminal, polyproline-rich repeat segment (Billuart *et al.*, 1998; Richnau and Aspenstrom, 2001; Nakano-Kobayashi *et al.*, 2009). Domain interactions of this BAR-RhoGAP subfamily have been previously described. For example, interactions have been identified between the C-terminal SH3BP1 (or 3BP1) proline-repeat

This article was published online ahead of print in MBoC in Press (http://www.molbiolcell.org/cgi/doi/10.1091/mbc.E12-07-0565) on December 5, 2012.

The authors declare no competing financial interests.

Address correspondence to: Céline DerMardirossian (dmceline@scripps.edu).

Abbreviations used: AD, Alzheimer's disease; APP, amyloid precursor protein; BAR, Bin-Amphyphysin-Rvs; BGIN, BARGIN; 3BP1 or SH3BP1, SH3-binding protein 1; CIN, chronophin; GAP, GTPase-activating protein; GFP, green fluorescent protein; GST, glutathione *S*-transferase; HD, Huntington's disease; LIMK, LIM kinase; mut, mutant; NOX, NADPH oxidase; ORF, open-reading frame; PAK, p21-activated kinase; PD, Parkinson's disease; PDXP, pyridoxal phosphatase; poly-Ub, poly-ubiquitin; rec, recoupling; ROS, reactive oxygen species; UTR, untranslated region; wt, wild type.

region and the SH3 domain of Abl kinase (Cicchetti *et al.*, 1992). It is unclear, however, how these interactions may influence 3BP1 RhoGAP or Abl kinase activity. Previous studies demonstrated a specificity of the 3BP1 GAP activity toward the inactivation of Rac1, Cdc42, and Tc10 RhoGTPases, with no influence on Rho activity in vitro (Cicchetti *et al.*, 1995). 3BP1 overexpression inhibits growth-factor-dependent cell ruffling, suggesting that 3BP1-mediated RhoGTPase inhibition can influence Rac1-dependent actin reorganization and consequent morphogenic changes (Cicchetti *et al.*, 1995). More recently, 3BP1 was shown to interact with members of the exocyst complex and to inactivate Rac1 at the leading edge to mediate cell morphogenic and migratory dynamics (Parrini *et al.*, 2011).

The 3BP1 gene locus resides on human chromosome 22, upstream of the haloacid dehydrogenase family phosphatase chronophin (CIN/PDXP), which was found to dephosphorylate pyridoxal phosphate (vitamin B6; Fonda, 1992) and the actin regulator cofilin (Gohla *et al.*, 2005; Huang *et al.*, 2008). Three distinct mRNA transcripts have been identified from these two gene loci: 1) a 3BP1 transcript comprising the entire exon complement of the 3BP1 gene locus, 2) the CIN phosphatase comprising two exons, and 3) an uncharacterized cDNA AK126873 identified in human brain, which combines exons from 3BP1 and CIN gene loci (Figure 1A).

Two unique features distinguish the AK126873 RhoGAP splice variant from its 3BP1 counterpart: 1) the second exon is excised from the N-terminal 3BP1 BAR domain, and 2) the terminal 3BP1 exon comprising the 3BP1 polyproline repeat region is replaced by the CIN second exon (Figure 1A). This results in an alternative splice product consisting of a modified N-terminal BAR domain, an intermediary RhoGAP domain, and a C-terminal partial CIN module. We named this alternative splice product BARGIN or BGIN to denote the unique sequential combination of BAR, RhoGAP, and CIN domains from 3BP1 and CIN gene loci. Most strikingly, BGIN is the only BAR-RhoGAP subfamily member that lacks a C-terminal polyproline-rich repeat region, which is replaced by the partial CIN phosphatase module.

It is still unclear how membrane compartmentalization of BAR-RhoGAP subfamily members is regulated and how these regulatory mechanisms might modulate RhoGTPase specifically at membrane platforms. BGIN interacts noncovalently with poly-ubiquitin chains through its C-terminus, which facilitates its distribution to membranes to mediate inactivation of a membrane-residing Rac1 population. This limits membrane-localized Rac1 effector function, such as the generation of reactive oxygen species (ROS) by the membrane-localized NADPH oxidase complex. BGIN/Ub interaction is also evident by coenrichment in Ub-enriched tangles in Alzheimer's disease (AD) brain and shows enhanced membrane distribution in AD tissue. BGIN depletion also elevates Rac1 activity and ROS generation with amyloid precursor protein (APP) proteotoxicity in an AD neuroblastoma model. BGIN/poly-Ub interactions may therefore serve to modulate Rac1 activity in response to Ub accumulation and proteotoxic stress.

RESULTS

BGIN is a unique RhoGAP component with a modified N-terminal BAR domain generated by alternative splicing in brain

A canonical dimethionine pair in the 3BP1 BAR domain initiates translation of the 3BP1 transcript (Supplemental Figure S1A). Excision of the second 3BP1 exon in the BGIN transcript shifts the 3BP1 dimethionine initiator sequence out of frame with respect to the BGIN open reading frame (ORF). No additional Met residues are encoded in-frame with the BGIN ORF in the BGIN 5′ untranslated region (UTR), thereby rendering the BGIN N-terminal sequence impossible to determine by simple bioinformatic sequence analysis.

Expression of C-terminal, green fluorescent protein (GFP)–tagged BGIN full-length or BAR domain constructs comprising the intact 5′ UTR produced a doublet, suggesting that BGIN translation was initiating at two sites (Supplemental Figure S1B). To identify putative initiation sites in the BGIN 5′ UTR, we purified the BGIN BAR domain construct expressed in HeLa cells and searched for peptides in the extreme N-terminus identified by mass spectrometry (Figure 1B). One peptide demarcated the minimal N-terminal BGIN BAR domain (Figure 1B, blue). Through mutagenesis of putative non-ATG start codons upstream of this peptide, we determined that a full-length BGIN product of 677 amino acids (aa; ~73.59 kDa) initiated from a CTG (Leu) codon and that a smaller BGIN isoform of 605 aa (66.19 kDa) was produced in HeLa cells by initiation from the first in-frame ATG (Met) with respect to the BGIN ORF (Supplemental Figure S1, C–F; see the Supplemental text). Initiation at the upstream CTG results in the recoding of a unique 42-aa N-terminal stretch with no homology to the 3BP1 N-terminal BAR domain (Supplemental Figure S1A).

We investigated genomic contiguity of 3BP1 and CIN/PDXP gene loci and CTG-mediated N-terminal BGIN initiation in various mammals (Table 1). 3BP1/CIN gene contiguity and splicing was predicted in many of these organisms (Table 1). However, recoding of the unique BGIN N-terminal region from an upstream CTG was only conserved between human, mouse, and chimpanzee (Table 1 and Figure 1C), suggesting that splicing of the BGIN N-terminus may be more limited to a select number of species.

Using affinity-purified antibodies recognizing the CIN C-terminal exon 2 module (Supplemental Figure S1G; see the Supplemental Methods), we observed CIN expression (31 kDa) in all tissue types with the CIN exon 2–specific antibody as described previously (Gohla *et al.*, 2005; Figure 1D). However, antibodies recognizing both the recoded BGIN$^{1\text{-}42}$ N-terminal region and CIN exon 2 module (Supplemental Figure S1G) revealed a band of ~74 kDa corresponding to full-length BGIN in brain tissue (Figure 1D and Supplemental Figure S1H). We also observed this band in cell lines of neuronal origin, such as Neuro 2A and SH-SY5Y neuroblastomas (Supplemental Figure S1I). Although we observe other bands around 74 kDa using the N-terminal BGIN antibody, these may be nonspecific bands that appear with long exposure (Supplemental Figure S1H). The absence of a smaller, 66.2-kDa BGIN form in brain suggested that initiation of the BGIN transcript in brain tissue efficiently uses the noncanonical CTG to generate a full-length BGIN product. We therefore exclusively use the full-length BGIN CTG-initiated isoform in all experiments from here on.

The CIN exon 2 domain (CIN aa 193–296/BGIN aa 574–677) comprises a partial CIN phosphatase module appended to the BGIN C-terminal end and lacks the catalytic D25 residue. Although this suggests that BGIN may not have an intrinsic function as a phosphatase, the placement of this domain at the C-terminus in place of the 3BP1 polyproline-rich region may indicate that this module possibly functions as a protein–protein docking module. We therefore purified hexahistidine (his_6)-tagged BGIN expressed in HeLa cells (see the Supplemental Methods) and identified ubiquitin (Ub) as a potential interacting component by mass spectrometry (Figure 1E).

The C-terminal CIN module is a poly-ubiquitin–binding module

To further investigate potential interactions between BGIN and Ub, we expressed glutathione *S*-transferase (GST) alone or GST-BGIN in

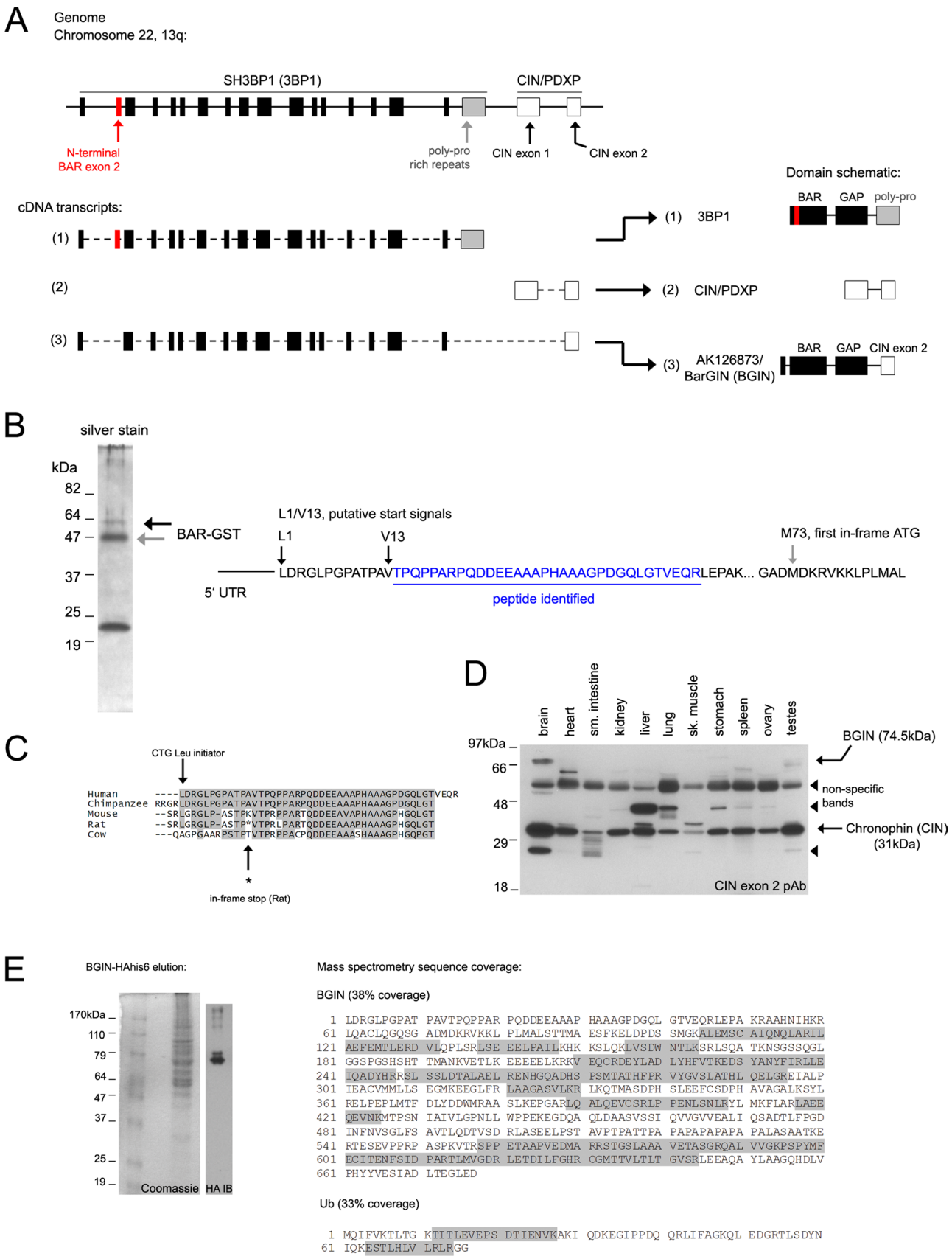

FIGURE 1: BGIN is an alternative splice product from SH3BP1/CIN loci and comprises a recoded N-terminal BAR domain. (A) Schematic of the human chromosome 22 SH3BP1/CIN locus. Three transcripts have been identified from this locus: 3BP1, CIN, and BGIN (AK126873). (B) Purification and sequence determination of the BGIN N-terminus. The BGIN BAR-domain doublet was expressed, purified, and subjected to mass spectrometry analysis. A peptide

Species	Chromosome number	Accession number			BGIN N-terminal CTG conservation
		3BP1	CIN/PDXP	BGIN C-terminal splice prediction	
Human	22	CR456576	BC000320	AK126873	
Rhesus monkey	10	XM_002798390[a]	Unavailable	XP_001088993	Unknown[b]
Chimpanzee	22	XM_515119[a]	Unavailable	XP_001161839	Conserved
Rabbit	Unknown	Unavailable	Unavailable	XP_002724386	Unknown[b]
Dog	10	Unavailable	Unavailable	XP_538386	Unknown[b]
Cow	5	XM_002687920[a]	NM_001035035	Unavailable	Nonconserved
Mouse	15	NM_020271[c]	NM_009164	Unavailable	Conserved
Horse	28	Unavailable	Unavailable	XP_001499590	Unknown[b]
Rat	7	XM_002729830	NM_001135819	Unavailable	Conserved, in-frame stop[d]

[a]Predicted mRNA sequence.
[b]Insufficient sequence information available for analysis.
[c]cDNA clone may be incomplete.
[d]Although the rat CTG is conserved, a stop codon is found in-frame downstream of the CTG.

TABLE 1: Evolutionary conservation of predicted BGIN N-terminal and C-terminal splicing properties.

HeLa cells under untreated conditions and in the presence of the proteasome inhibitor MG132 to elevate cellular poly-Ub levels and immunoblotted for Ub in GST precipitates. BGIN weakly coprecipitated with a high–molecular weight poly-Ub smear under steady-state conditions, which was greatly enhanced with MG132 (Figure 2A). To determine whether the CIN exon 2 module (BGIN$^{574-677}$, which we refer to as CIN exon 2 from here on), was required for poly-Ub interaction, we precipitated GST-tagged BGIN deletion constructs and assayed for poly-Ub interaction in the presence and absence of MG132 (Figure 2B). BGIN constructs lacking the CIN exon 2 domain were unable to coprecipitate with poly-Ub, whereas the CIN exon 2 module alone demonstrated efficient poly-Ub interactions under steady-state conditions, with enhanced interactions upon MG132 treatment (Figure 2B). Moreover, whereas BGIN/poly-Ub interactions gradually increased with MG132 treatment, 3BP1 failed to bind poly-Ub under all conditions tested (Supplemental Figure S2A).

BGIN did not appear to be covalently tagged with degradatory-targeting poly-Ub linkages since BGIN immunoblots (GST blots) did not mirror higher–molecular weight smears seen in duplicate Ub blots (Figure 2A). We observed that increasing concentrations of SDS dissociated poly-Ub from CIN exon 2 precipitates, supporting the notion that BGIN/poly-Ub interactions occur noncovalently (Supplemental Figure S2B). Furthermore, the CIN exon 2 module comprises a single Lys residue (K594) available for poly-Ub conjugation. Mutation of this residue to Arg (K594R) had no effect on poly-Ub coprecipitation with CIN exon 2 (Supplemental Figure S2C), indicating that CIN exon 2 and poly-Ub interact through noncovalent association.

We found that CIN exon 2 coprecipitates with long poly-Ub conjugates from HeLa and Neuro 2A cells (Supplemental Figure S2D) with little or no interaction with mono-Ub in vivo. We also reconstituted CIN exon 2/poly-Ub interactions in vitro by coprecipitating increasing amounts of purified GST or GST-CIN exon 2 with purified his_6myc poly-Ub (Supplemental Figure S2E). Although CIN exon 2 coprecipitated with purified poly-Ub, no coprecipitation was observed with GST alone (Supplemental Figure S2E). Of interest, CIN exon 2 coprecipitated preferentially with higher–molecular weight poly-Ub conjugates, where no Ub monomers were detected in these pull-down assays (Supplemental Figure S2E). This suggests that the CIN exon 2 module interacts selectively with polyconjugated Ub chains. Although these results indicate a bias for CIN exon 2 interaction with polyconjugated Ub, we do not discount the possibility that low-affinity interactions with mono-Ub might not be detected using these interaction assays.

We then investigated whether modulating linear poly-Ub chain length could influence BGIN C-terminus/Ub interactions in vitro. We purified recombinant his_6-tagged linear poly-Ub of varying lengths and assayed these constructs for coprecipitation with recombinant GST-CIN exon2 by GST pull-down. Recombinant di-Ub (Ub2) failed to show interaction with GST-CIN exon 2, whereas penta-Ub coprecipitated with GST-CIN exon 2 (Supplemental Figure S2F). We also observed weak association of recombinant tetra-Ub with GST-CIN exon 2, suggesting that Ub/CIN exon 2 interactions may be dependent on Ub chain length. To confirm this, we purified recombinant GST-linked Ub chains of varying lengths and performed GST pull-down assays with recombinant purified GFP-tagged CIN exon 2.

demarcating the minimal BGIN N-terminal BAR region was identified (blue sequence), and potential non-AUG initiation codons upstream are indicated. (C) The recoded N-terminal BGIN BAR region is conserved among various mammalian species. CLUSTALW alignment of the recoded reading frame from the CUG (L) start signal between the species indicated; an in-frame stop was detected within this sequence in rat. (D) Multiple tissue Western blots (IMGENEX) were probed with a C-terminal (CIN exon 2) BGIN/CIN antibody. The CIN exon 2 antibody detects both BGIN (73.59 kDa) and CIN (31 kDa). Arrowheads indicate nonspecific bands. (E) Identification of Ub in BGIN complexes by mass spectrometry. BGIN-HAhis_6 was purified as described in the Supplemental Methods, and elutions were resolved by SDS–PAGE and stained with Coomassie blue or immunoblotted for HA. Peptides identified for BGIN or Ub in BGIN eluates by mass spectrometry are indicated in gray.

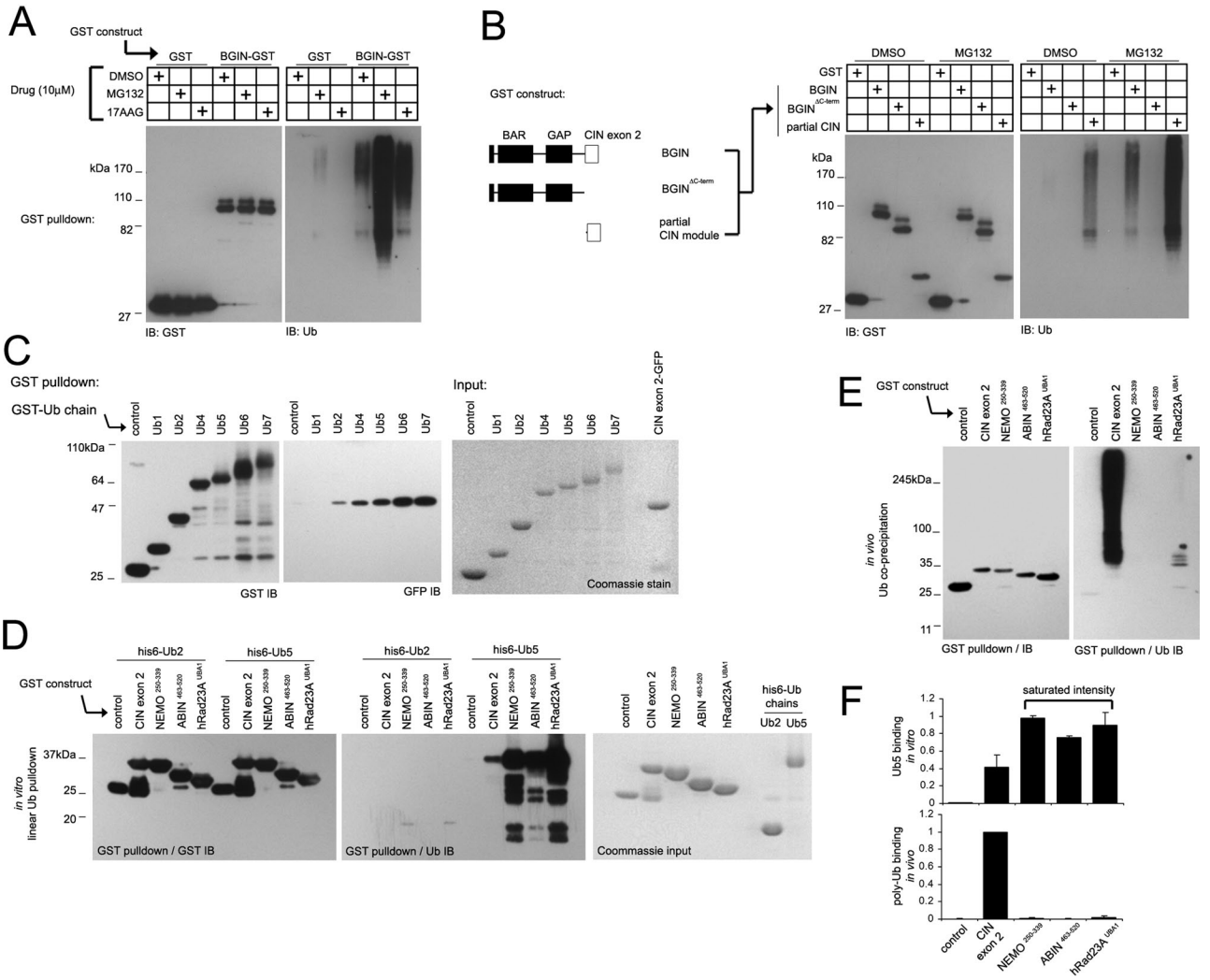

FIGURE 2: BGIN interacts with poly-ubiquitin through the CIN exon 2 module. (A) HeLa cells were transfected with GST or BGIN-GST constructs and treated with dimethyl sulfoxide (DMSO) or 10 μM MG132 or 17AAG for 5 h, and GST precipitates generated from lysates were immunoblotted for GST or Ub. (B) GST-tagged BGIN constructs were expressed in HeLa cells, and GST precipitates were generated from cells treated with DMSO or MG132 (5 μM, 5 h). Precipitates were immunoblotted for GST or Ub. (C) Recombinant purified GST-Ub chains of the indicated lengths were incubated with recombinant purified CIN exon 2-GFP and precipitated with glutathione–Sepharose. Right, Coomassie stain of the binding reaction input. (D–F) Comparison of Ub-binding modules in vitro and in vivo. (D) A 20-μg amount of recombinant GST-tagged Ub-binding domains immobilized on glutathione–Sepharose was incubated with 20 μg of his_6-Ub2 or Ub5, precipitated, and analyzed for GST/Ub by immunoblot. Right, Coomassie stain of binding inputs. (E) GST-tagged Ub-binding domains in pRK5 were transfected into HeLa cells, precipitated with glutathione–Sepharose, and analyzed for GST/Ub. (F) Graphs represent relative Ub binding in vitro (top) and in vivo (bottom; highest value set to 1.0) from two experiments (mean ± SD). Saturated band intensity with Ub5 in vitro binding as indicated will diminish differences detected in CIN exon 2 interactions compared with other Ub-binding domains.

Similarly, we also observed little or no binding with mono/di-Ub chains, with incrementally improved binding with Ub4 to Ub7 chains (Figure 2C).

We compared binding affinities of the CIN exon 2 domain with other ubiquitin modules, including UBAN motifs from Nemo1 and Abin1, and the hRad23 UBA domain (Dikic *et al.*, 2009). Using recombinant purified GST-tagged Ub-binding domains immobilized to glutathione beads, we found that the CIN exon 2 domain exhibited much weaker binding to recombinant linear Ub5 chains in vitro (Figure 2D). In vivo, we found that only the CIN exon 2 domain exhibited robust interactions with a poly-Ub smear (Figure 2E). Because Ub can form polyconjugate chains through seven possible lysines within the Ub sequence, we determined the poly-Ub chain type copurified with the CIN exon 2 domain in vivo through the identification of diglycine-tagged lysines on Ub in CIN exon 2 precipitates by mass spectrometry (Supplemental Figure S2G). We identified three peptides that confirmed K29 and K48 poly-Ub linkages, which were present in CIN exon 2 precipitates (Supplemental Figure S2H). Although we cannot currently exclude the possibility of interaction with other poly-Ub chain types, this suggests that CIN exon 2 interacts with endogenous K29 and K48 poly-Ub chains in vivo. We then reevaluated CIN exon 2 poly-Ub interactions in vivo in comparison to the K48-linkage–specific UBA domain of *Schizosaccharomyces pombe* MUD1 (Komander *et al.*, 2009). NEMO/Abin1 UBAN and hRad23A UBA largely failed to precipitate poly-Ub, whereas CIN exon 2 and MUD1 UBA pulled down poly-Ub from

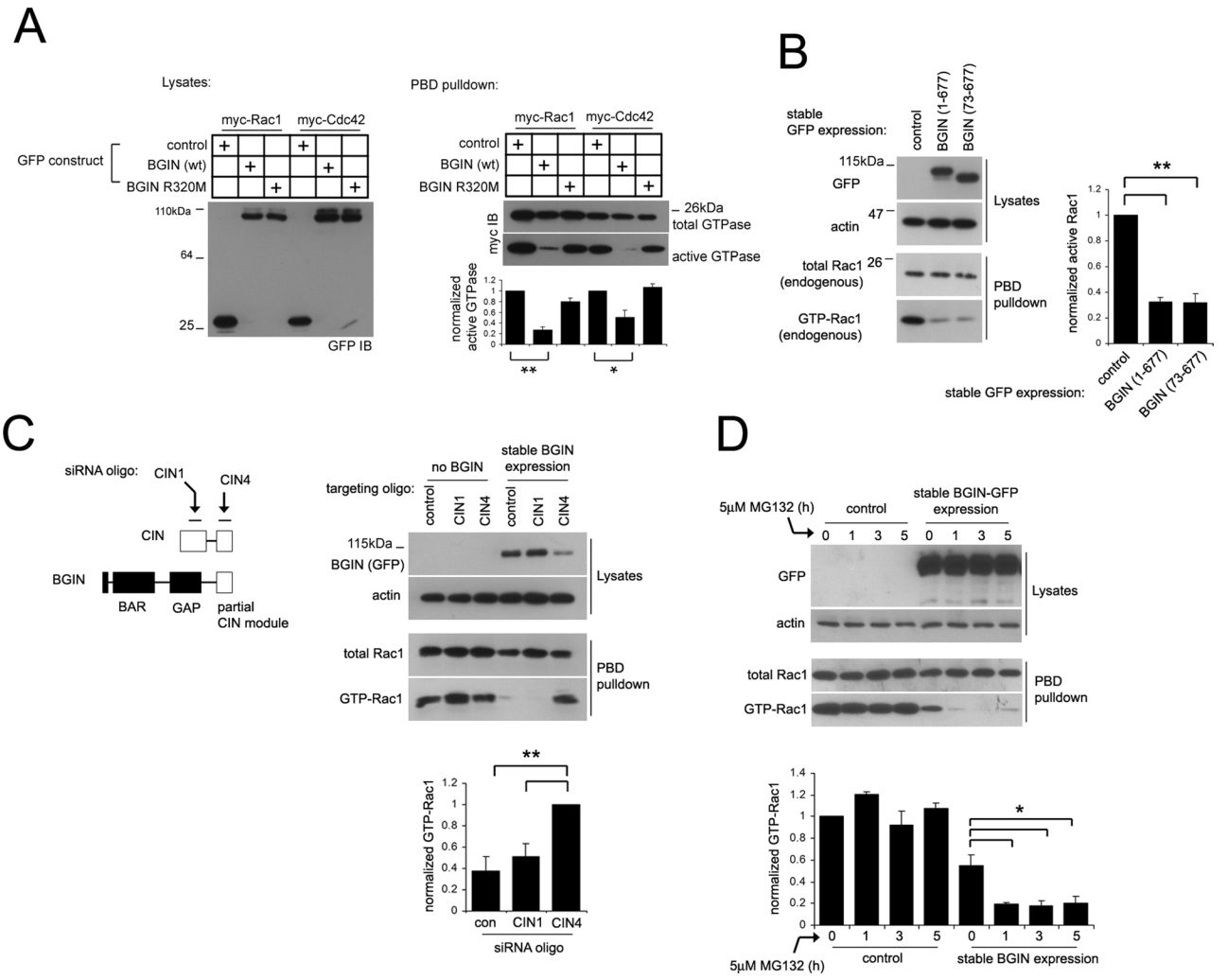

FIGURE 3: MG132 enhances BGIN-dependent Rac1 inactivation. (A) BGIN expression enhances Rac1/Cdc42 inactivation. Myc-tagged Rac1 or Cdc42 was coexpressed with GFP-tagged BGIN wild-type or R320M constructs in HEK293T cells as indicated, and lysates were subjected to PBD-GST pull-down. Lysates were immunoblotted for GFP and myc-GTPase expression, and PBD-GST precipitates were immunoblotted for GTP-loaded myc-Rac1/Cdc42. (B) Stable BGIN expression inactivates Rac1. Lysates from HeLa cells stably expressing long or short GFP-tagged BGIN isoforms were subjected to PBD pull-down assays. (C) Schematic of BGIN siRNA-targeting oligos. Control HeLa cells or BGIN-expressing clones were transfected with control, CIN1, or CIN4 siRNA oligos as indicated, and GTP-Rac1 was assayed by PBD pull-down assay. (D) BGIN expression results in MG132-responsive Rac1 inactivation. Control or stably expressing BGIN-GFP HeLa cells were treated with MG132 for the time indicated, and Rac1-GTP was quantified by PBD pull-down assay. All graphs displayed (A–D) depict Rac1-GTP levels normalized for total Rac1 and compiled from a minimum of three experiments (mean ± SEM, $^{**}p < 0.006$, $^{*}p < 0.05$).

HeLa cell lysates (Supplemental Figure S2I). These results suggest that Ub-linkage binding specificity can influence steady-state poly-Ub/CIN exon 2 interactions in vivo.

Taken together, these results indicate that the BGIN C-terminal CIN exon 2 domain is a poly-Ub–binding module that selectively binds poly-Ub chain linkages.

MG132 treatment enhances BGIN-dependent Rac1 inactivation

Next we determined whether poly-Ub accumulation could influence BGIN-dependent Rac1 inactivation. Similar to previous reports indicating that 3BP1 mediates specific GTPase-activating activity toward Rac1 and Cdc42 (Cicchetti *et al.*, 1995), wild-type BGIN inactivated both Rac1 and Cdc42 by PBD pull-down assay (Benard *et al.*, 1999; Stofega *et al.*, 2006; see the Supplemental Methods; Figure 3A). Moreover, mutation of the critical Arg residue (R320M, which is analogous to the 3BP1 R312 residue; Supplemental Figure S3A) within the GAP domain rendered BGIN inactive toward Rac1 and Cdc42 substrates (Figure 3A). Stable BGIN expression also reduced Rac1-GTP levels in comparison to the parental HeLa cell line, and both long ($BGIN^{1-677}$) and short ($BGIN^{73-677}$) BGIN isoforms had equivalent effects in reducing bulk Rac1 activity (Figure 3B). Rac1-GTP levels were restored by depletion of exogenous BGIN with BGIN-targeting oligos (CIN4), with little or no influence from the nontargeting control and CIN1 oligos (Figure 3C). These results demonstrate that BGIN is a GAP for Rac1 and that perturbations in BGIN levels can influence Rac1 activity.

We then determined the effect of MG132 treatment on BGIN-dependent Rac1 inhibition. MG132-induced Rac1 inactivation in BGIN-GFP–expressing clones, where little or no effect was

observed in the parental cell line (Figure 3D). We also tested whether similar Rac1 inactivation can be observed in a neuronal cell type such as SH-SY5Y expressing BGIN (Supplemental Figure S1I). We also find a slight attenuation of Rac1 activity in SH-SY5Y cells with MG132 treatment (Supplemental Figure S3B). Conversely, depletion of BGIN increased active Rac1 levels in whole-cell lysates and rendered Rac1-GTP levels unresponsive to MG132 treatment (Supplemental Figure S3C). Taken together, these results indicate that BGIN GAP activity is enhanced with MG132 treatment and can act as a signal relay mechanism to potentially inactivate Rac1 during poly-Ub accumulation. In all assays just described, treatment with 5 μM MG132 for 5 h failed to influence BGIN stability (Figure 3D and Supplemental Figure S3, C and D), suggesting that BGIN/poly-Ub interactions might act to modulate functional BGIN activity by a means other than its total abundance or stability.

Poly-Ub/BGIN interactions promote BGIN distribution to membranes

Membrane-associated Rac1 activation is essential to the activation of downstream effector systems such as the p21-activated kinases (PAKs), WAVE, and ROS generation through the NADPH complex (Nox1; Bokoch, 2003; Jaffe and Hall, 2005). We therefore determined whether BGIN could distribute to biochemical membrane fractions. Full-length, GST-tagged BGIN or individual BAR, GAP, or CIN exon 2 expressed in HeLa cells were subjected to biochemical membrane/cytosol fractionation, and GST immunoblots of cytosol or membrane fractions were run alongside an incremental GST reference (Supplemental Figure S3, E and F). Approximately 15% of full-length BGIN distributed to membranes, whereas the BAR and GAP domains alone distributed very poorly to membranes (<5%; Supplemental Figure S3, F and G). The CIN exon 2 domain alone, however, was found to distribute efficiently to membranes (~13%), suggesting that the CIN exon 2 domain may have a primary role in mediating BGIN distribution to membranes.

We also determined the subcellular distribution of endogenous Ub by biochemical fractionation in HeLa cells. Ubiquitin monomers exclusively appeared in cytosolic fractions, whereas high–molecular weight poly-Ub chains appeared primarily in detergent-soluble membrane fractions (Supplemental Figure S3H). Because we did not observe significant changes in homotypic BGIN dimer interactions through its BAR domain with MG132 (Figure S3, I and J), the possibility arises that BGIN might distribute to membranes through poly-Ub/CIN exon 2 docking.

Membrane-associated BGIN was incrementally boosted with MG132 treatment in both stably expressing (Figure 4A) and transiently transfected HeLa cells (Supplemental Figure S4A), indicating that BGIN distribution to membranes can be influenced by poly-Ub accumulation. Moreover, Rac1 was exclusively distributed to cytosolic/membrane fractions and exhibited little change with MG132 treatment (Figure 4A, adjacent line graphs). This suggests that BGIN/poly-Ub interactions might serve to bring BGIN in proximity to a membrane-resident Rac1 population.

We then investigated the effects of uncoupling poly-Ub/BGIN interactions on BGIN subcellular distribution. To this end, we generated BGIN CIN exon 2 alleles ($BGIN^{576\text{-}677}$) that abrogated BGIN/poly-Ub binding. We screened a library of 184 CIN exon 2 module ($BGIN^{576\text{-}677}$) clones for loss of poly-Ub–binding capacity by GST pull-down assay and obtained eight alleles comprising a combination of 7 to 16 missense mutations that rendered them refractory to poly-Ub binding (see the Supplemental Methods and Supplemental Figure S4, B and C). We subcloned three CIN exon 2 alleles (mut159, 167, and 168) into full-length BGIN and confirmed that the allelic variants lacked the capacity to bind poly-Ub in the absence or presence of MG132 (Figure 4B). We selected two redundant poly-Ub nonbinding alleles (mutants 159 and 167) comprising the lowest mutation complement for further study.

GST-tagged wild-type and mutant BGIN isoforms were expressed in HeLa cells, and their abundances in cytosolic, membrane, and insoluble fractions were determined under steady-state and MG132-treated conditions (Figure 4C). Of interest, non-poly-Ub–binding BGIN variants largely failed to partition to both detergent-soluble membrane and insoluble fractions in comparison to wild-type BGIN under both steady-state and MG132-treated conditions (Figure 4C), where little difference was seen in cytosolic abundance of wild-type and mutant BGIN alleles. Taken together, these results indicate that interactions between poly-Ub and the BGIN C-terminus can enhance BGIN distribution to membranes.

We also observed distinctive differences in cell morphology and spreading with stable expression of BGIN wild-type and mut159 (poly-Ub nonbinding) alleles in HeLa cells. HeLa cells are multipolar and typically spread with numerous F-actin–rich apexes (Figure 4D). Whereas expression of the mut159 allele also results in a multipolar phenotype, expression of wild-type BGIN produces cells that are often elongated and primarily bipolar (Figure 4D).

Rac1 activation correlates with lamellipodial protrusion during plating on substrates such as fibronectin (Price *et al*., 1998). We therefore investigated whether expression of wild-type or mut159 BGIN alleles affected cell spreading (see the Supplemental Methods). Wild-type BGIN attenuated cell spreading after 45 min plating on fibronectin, whereas the mut159 allele had little effect on spreading (Figure 4E). It is striking that many of the mut159 cells protruded with a thick lamellipodial layer similar to cells transfected with the active Rac1 Q61L allele (Figure 4E).

Taken together, these results indicate that BGIN can modulate Rac1-dependent morphology and that alteration of CIN exon 2 functionality (such as poly-Ub binding) can perturb BGIN function.

BGIN/poly-Ub interactions attenuate membrane-associated Rac1 activity

Having demonstrated that uncoupling BGIN/poly-Ub interactions can influence subcellular BGIN distribution to membranes, we investigated whether these mutant alleles could influence cellular Rac1 activity. Using PBD pull-down assays (see the Supplemental Methods), we found that transient HEK293T transfection or stable HeLa transfection of BGIN wild-type, mut159, or mut167 alleles had comparable effects in reducing total Rac1 activity (Figure 5A, left, and Supplemental Figure S5A, left). However, whereas wild-type BGIN attenuated membrane-associated Rac1 activity, mut159 and mut157 alleles inactivated Rac1 less efficiently (Figure 5A, right, and Supplemental Figure S5A, right), which correlated with their comparatively poor distribution to membranes (Figure 5A). We also investigated whether BGIN wild-type or mut159 alleles had equivalent effects in distribution and membrane Rac1 activity in a neuronal cell line (Neuro 2A cells). Similarly, BGIN mut159 distributed poorly to membranes in Neuro 2A cells, resulting in attenuated Rac1 inactivation compared with wild-type BGIN (Supplemental Figure S5, B and C). Wild-type BGIN also reduced membrane-associated Cdc42 activity with minimal influence on RhoA activation, whereas mut159 expression had comparatively little effect on Cdc42 inactivation (Supplemental Figure S5D).

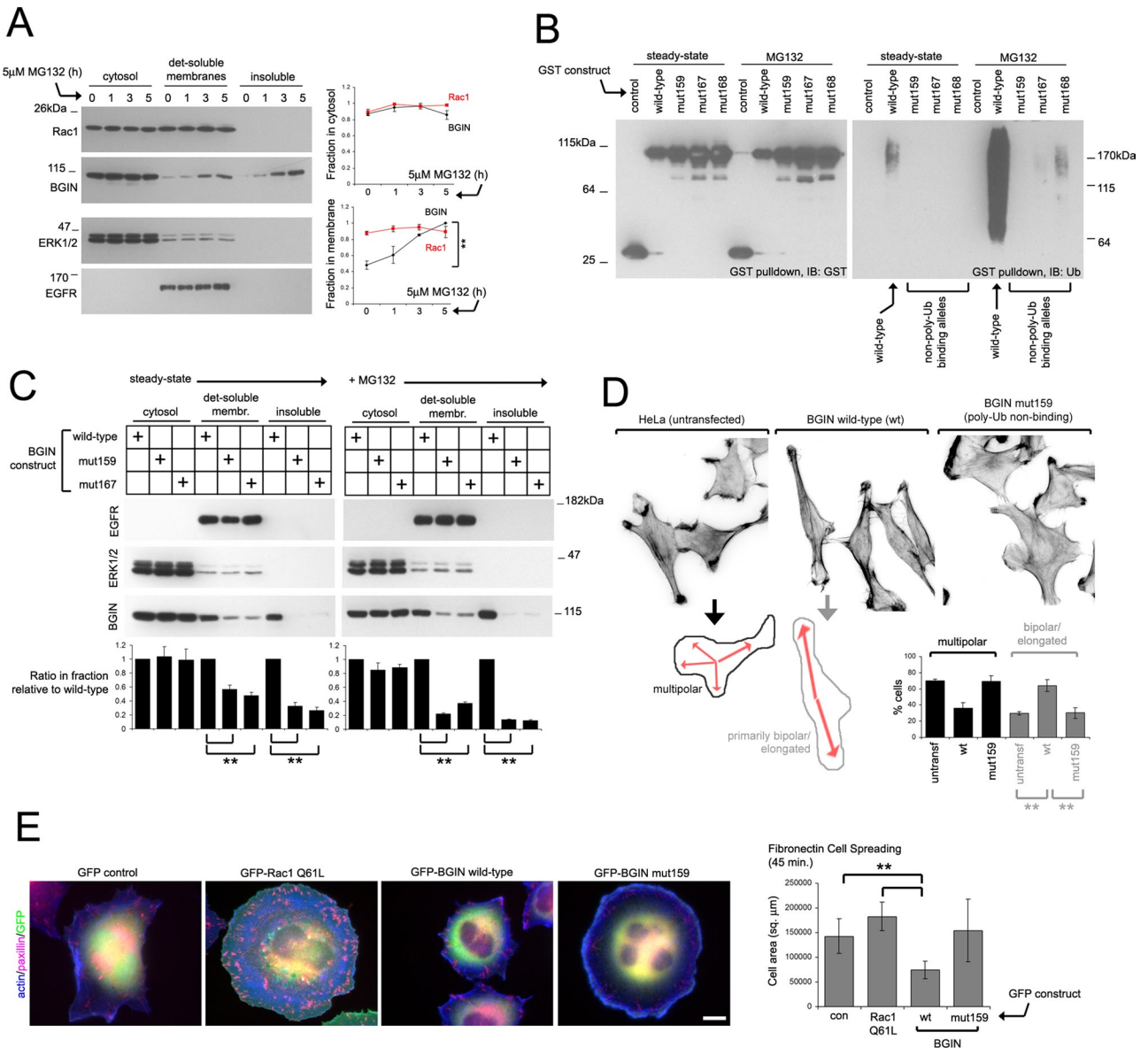

FIGURE 4: Interactions between BGIN and poly-ubiquitin promote BGIN partitioning to membrane fractions. (A) Poly-ubiquitin accumulation triggers BGIN distribution to detergent-soluble membrane fractions. Stably expressing BGIN-GFP HeLa cells were treated with MG132, and lysates were separated into cytosolic and detergent-soluble/insoluble membrane fractions. Quantification of Rac1 in cytosolic and detergent-soluble membrane fractions are presented as mean ± SEM from three independent experiments, where the peak intensity is set to 1.0 (**$p < 0.001$). (B) CIN exon 2 mut159, 167, and 168 alleles were subcloned into full-length GST-BGIN constructs, expressed in HeLa cells, and assayed for poly-Ub interactions under steady-state and presence of MG132 (5 μM, 5 h) by GST pull-down assay. (C) GST-tagged wild-type BGIN and two poly-Ub refractory mutants (mut159 and mut167) from B were expressed in untreated or MG132-treated (5 μM, 5 h) HeLa cells and separated into the subcellular fractions indicated. Equal protein quantities were immunoblotted from each fraction and quantified as a ratio in comparison to the wild-type BGIN (set to 1.0). Values of mean ± SEM from three independent experiments are presented (**$p < 0.003$). (D) Morphology of cells stably expressing wild-type or mut159 BGIN-GFP. A total of 10^5 cells seeded on 15-mm coverslips were stained for F-actin and scored for a multipolar morphology (more than two apexes) or an elongated/bipolar phenotype (primarily two apexes). Infrequent appearance of rounded cells were excluded from scoring. Images shown are inverted phalloidin-stained images. The graph displayed are cumulative percentages of multipolar/bipolar cells from four experiments (mean ± SD, **$p < 0.0005$). (E) Cell spreading on fibronectin. HeLa cells transiently expressing GFP alone or constitutively active GFP-Rac1 Q61L or stably expressing wild-type or mut159 BGIN-GFP were seeded onto 0.0001% fibronectin coverslips for 45 min and costained for actin and paxillin. Total cell area was measured under each condition from three independent experiments (mean ± SD shown in the adjacent graph, **$p < 3 \times 10^{-9}$).

We then investigated whether recoupling poly-Ub to the non-poly-Ub–binding mut159 allele (Figure 5B) could reestablish membrane distribution and membrane-specific Rac1 inactivation. We determined the minimal combination of reversion mutations in the mut159 allele (Figure 5B) to reestablish poly-Ub interactions in three steps: 1) We found that no single mut159 residue reversion restored

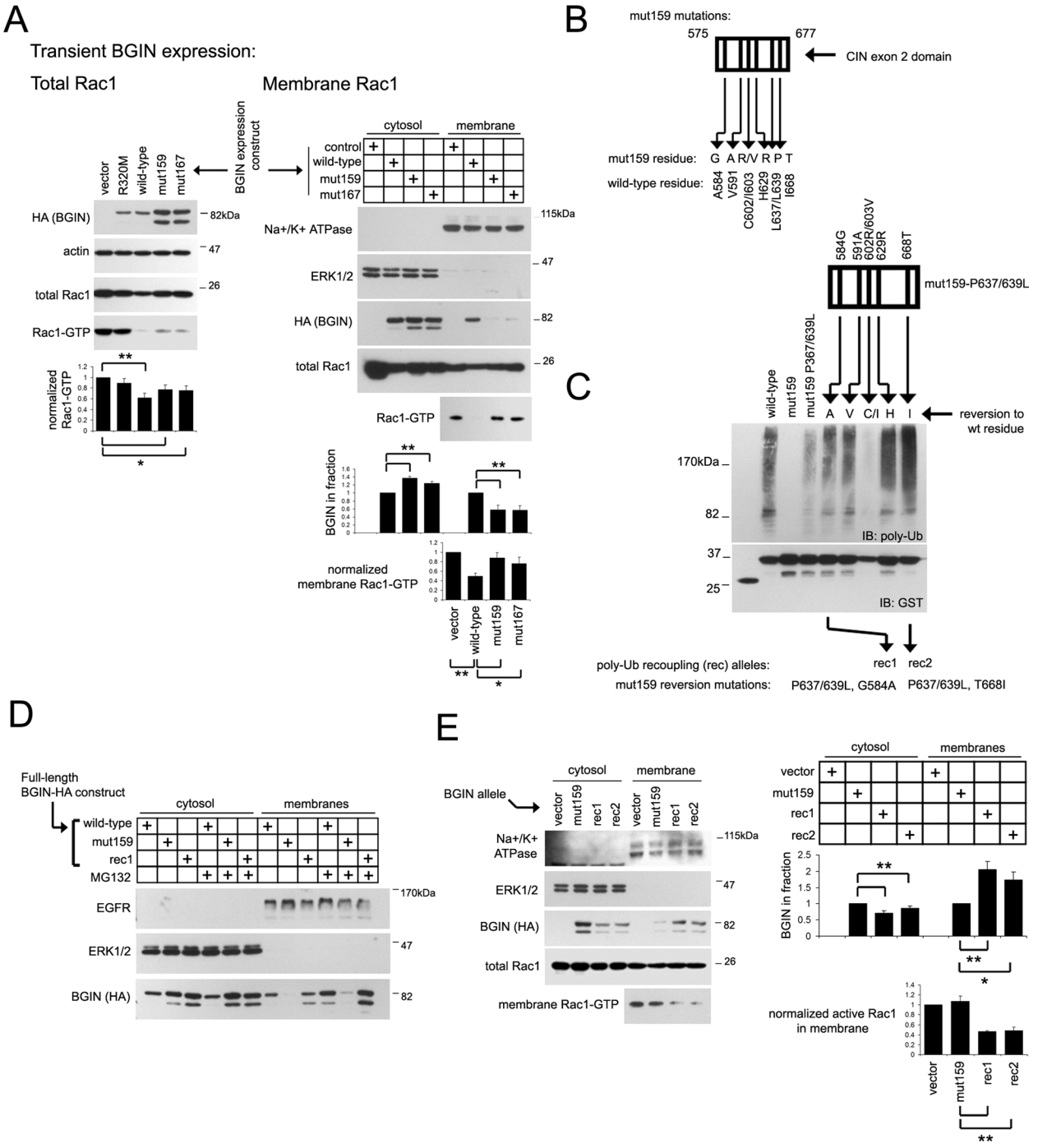

FIGURE 5: Interactions with poly-Ub promote BGIN-mediated Rac1 inactivation at the membrane. Uncoupling poly-Ub interactions attenuates BGIN-dependent Rac1 inactivation. (A) HEK293T cells coexpressing the myc-Rac1 and BGIN-HA constructs indicated were subjected to PBD pull-down assay as described in the Supplemental Methods to determine total (left) or membrane-specific Rac1-GTP levels (right). Graphs depict BGIN levels normalized to wild-type BGIN (set to 1.0) or normalized Rac1-GTP levels from four experiments (mean ± SEM, $*p < 0.05$, $**p < 0.005$). (B) Schematic of mutated residues in the mut159 allele within the BGIN aa 575–677 region. (C) Reversion scheme of the mut159 allele. The mut159 allele with an L637/639P reversion pair was coupled to an additional reversion to wild-type residue, and GST-tagged $BGIN^{575-677}$ constructs were assayed for poly-Ub recoupling. Two mut159 mutational reversion combinations demonstrating poly-Ub recoupling, rec1 (P637/639L, G584A) and rec2 (P637/639L, T668I), were selected for further analysis. (D) Recoupling BGIN/poly-Ub interactions restores BGIN membrane distribution. HeLa cells were transfected with HA-tagged full-length BGIN wild-type, mut159, or rec1 alleles, treated with 5 μM MG132 for 5 h as indicated, and subjected to cytosol/membrane fractionation and analysis by immunoblotting. (E) Recoupling BGIN/poly-Ub interactions restores BGIN-dependent Rac1 inhibition in detergent-soluble membranes. HEK293T cells coexpressing myc-Rac1 and the full-length HA-tagged BGIN constructs were subjected to membrane fractionation and PBD pull-down assay as described in *Materials and Methods*. Quantification of BGIN in cytosol and membrane fractions and normalized membrane Rac1-GTP levels are shown as averages ± SEM of four experiments ($**p < 0.006$, $*p < 0.02$).

poly-Ub interactions (Supplemental Figure S5E), 2) a P637L/P639L reversion pair partially restored poly-Ub binding (Supplemental Figure S5F), and 3) reversion of a third mut159 residue (G584 or T668) in addition to P637L/P639L could restore mut159 poly-Ub interactions to wild-type levels (Figure 5C). We refer from here on to P637L/P639L, G584A and P637L/P639L, T668I mut159 reversion combinations as "rec1" and "rec2" poly-Ub recoupling alleles, respectively (Figure 5C). Placed in the context of full-length GST-BGIN, rec1 and 2 alleles reestablished poly-Ub interactions in the presence of MG132, whereas mut159 remained unable to bind poly-Ub by GST pull-down assay (Supplemental Figure S5G).

Both wild-type and rec1 full-length BGIN constructs partitioned to membrane fractions under steady-state conditions, with enhanced membrane distribution upon MG132 treatment (Figure 5D). The mut159 allele, however, largely failed to partition to membrane fractions, even in the presence of MG132 (Figure 5D), demonstrating a direct correlation between poly-Ub/BGIN interactions and subcellular BGIN distribution to membranes. We also found that CIN exon 2 alone in the absence of BAR and GAP domains distributes to membrane fractions (Supplemental Figure S5H), suggesting that this domain is sufficient to dock protein components to membranous compartments through poly-Ub interactions. Similar to mutant alleles in their full-length contexts, membrane partitioning of the CIN exon 2 domain was dependent on poly-Ub binding (Supplemental Figure S5H). Ub-binding domains such as NEMO and Abin1 UBAN motifs or the hRad23A UBA1 domain also partitioned poorly to membranes in comparison to CIN exon 2, indicating that membrane partitioning may be a distinct property of the CIN exon 2 domain (Supplemental Figure S5I).

We then determined the effect of poly-Ub recoupling on membrane-specific Rac1 activity in HEK293T cells. Transient transfection of both poly-Ub rec1 and rec2 recoupling alleles could restore BGIN membrane distribution and attenuate membrane-specific Rac1-GTP levels in comparison to the mut159 allele (Figure 5E). Taken together, these results indicate that poly-Ub interactions with BGIN promote BGIN distribution at the plasma membrane and BGIN-dependent attenuation of a membrane-bound Rac1 population.

Poly-Ub/BGIN interactions attenuate ROS generation through the Nox1 complex

Because Rac1 and Rac2 are essential activating components of membrane-associated NADPH oxidase 1/2 (Nox1/Nox2) enzyme complexes, respectively, which facilitate extracellular ROS generation (Knaus *et al*., 1991; Bedard and Krause, 2007), we examined how BGIN/poly-Ub interactions could possibly influence Rac1/Nox1-dependent ROS generation (Figure 6A). Using an established HEK293T expression system to assay Nox1-dependent ROS generation (see the Supplemental Methods), we confirmed that exogenous expression of Nox1, NoxA1, and NoxO1 components generated ROS as assayed by chemiluminescence assay, with little or no ROS generated by single transfection of these components alone (Supplemental Figure S6A). ROS generation using this system was sensitive to Rac1 inactivation, as overexpression of a dominant-negative T17N Rac1 construct also inhibited Nox1-dependent ROS generation (Supplemental Figure S6B).

We then determined whether BGIN-dependent Rac1 inactivation could influence ROS generation (Figure 6A, model). Incremental BGIN expression caused a corresponding decrease in ROS generation (Supplemental Figure S6C), suggesting that BGIN-dependent Rac1 inhibition could attenuate Nox1-dependent ROS production. Indeed, although additional expression of wild-type BGIN reduced ROS generation to ~50% in Nox1/A1/O1 transfected cells, expression of R320M BGIN constructs lacking GAP activity failed to influence ROS production (Supplemental Figure S6D).

Because BGIN membrane distribution was found to be dependent on poly-Ub interactions, we determined whether uncoupling and recoupling poly-Ub to BGIN could influence ROS generation. Expression of mut159 and mut167 non-poly-Ub–binding alleles had surprisingly little influence on Nox1-dependent ROS generation in comparison to wild-type BGIN (Figure 6B). Moreover, poly-Ub–recoupling alleles rec1 and rec2 restored BGIN-mediated inhibition of Nox1-dependent ROS generation (Figure 6C), demonstrating that poly-Ub interactions contribute significantly to BGIN-dependent attenuation of Nox1 ROS generation.

Perturbation of BGIN levels also induced changes in ROS generation in SH-SY5Y cells. Stable expression of BGIN induced a reduction in ROS output in comparison to untransfected controls (Supplemental Figure S6E). Using the CIN4 siRNA oligo to deplete BGIN in SH-SY5Y cells (Figure 6D), we also observed a slight increase in ROS generation compared with nontargeting control and CIN1 siRNA oligos (Figure 6E).

Based on the use ROS generation as a membrane-associated Rac1 effector system, these results indicate that BGIN/poly-Ub interactions can work to limit downstream Rac1 signaling determinants at the membrane.

Screening Ub-related neurodegenerative proteinopathies for Ub/BGIN aggregate interactions and differential BGIN distribution

Transient BGIN overexpression in HeLa cells yielded distinctive perinuclear tubule-shaped aggregates in a small proportion of transfected cells (~10%; see the Supplemental Methods and Supplemental Figure S6F). Furthermore, localization of BGIN in perinuclear clusters was dependent on the BGIN CIN exon 2 domain: constructs lacking this domain completely were unable to form perinuclear tubule clusters, and the BGIN C-terminal CIN exon 2 domain alone formed smaller but distinctive perinuclear granules (Supplemental Figure S6F). Although these perinuclear BGIN clusters did not colocalize with markers for perinuclear compartments such as the endoplasmic reticulum–Golgi intermediate compartment (ERGIC) or Golgi (not shown), we found an enrichment of Ub within these perinuclear clusters (Figure 6F). Of interest, elevating cellular poly-Ub levels through MG132 treatment increased the abundance of cells with these perinuclear BGIN clusters, where no aggregates were found in BGIN constructs lacking the CIN exon 2 domain, indicating that BGIN aggregation may be potentially influenced by poly-Ub/CIN exon 2 interactions and poly-Ub accumulation (Supplemental Figure S6G).

We find the appearance of BGIN in Ub-enriched aggregates interesting, as Ub aggregates in neurodegeneration is commonplace and correlates with neurodegenerative decline in age-related disorders such as AD, Parkinson's disease (PD), and Huntington's disease (HD; Alves-Rodrigues *et al*., 1998). Proteasomal dysfunction and poly-Ub accumulation are common themes among these disorders, with the manifestation of distinct Ub-associated aggregate pathologies appearing in late neurodegenerative onset. Given that our results indicate that BGIN aggregation can be influenced by poly-Ub accumulation (Supplemental Figure S6G), we tested for potential BGIN/Ub interaction through their coaggregation in Ub-enriched inclusions in AD, PD, and HD disorders by immunohistochemistry. This may potentially indicate whether proteotoxicity in AD, PD, or HD can influence BGIN/Ub interactions and influence BGIN/Rac1 signaling (Supplemental Figure S7A). Because BGIN accumulation

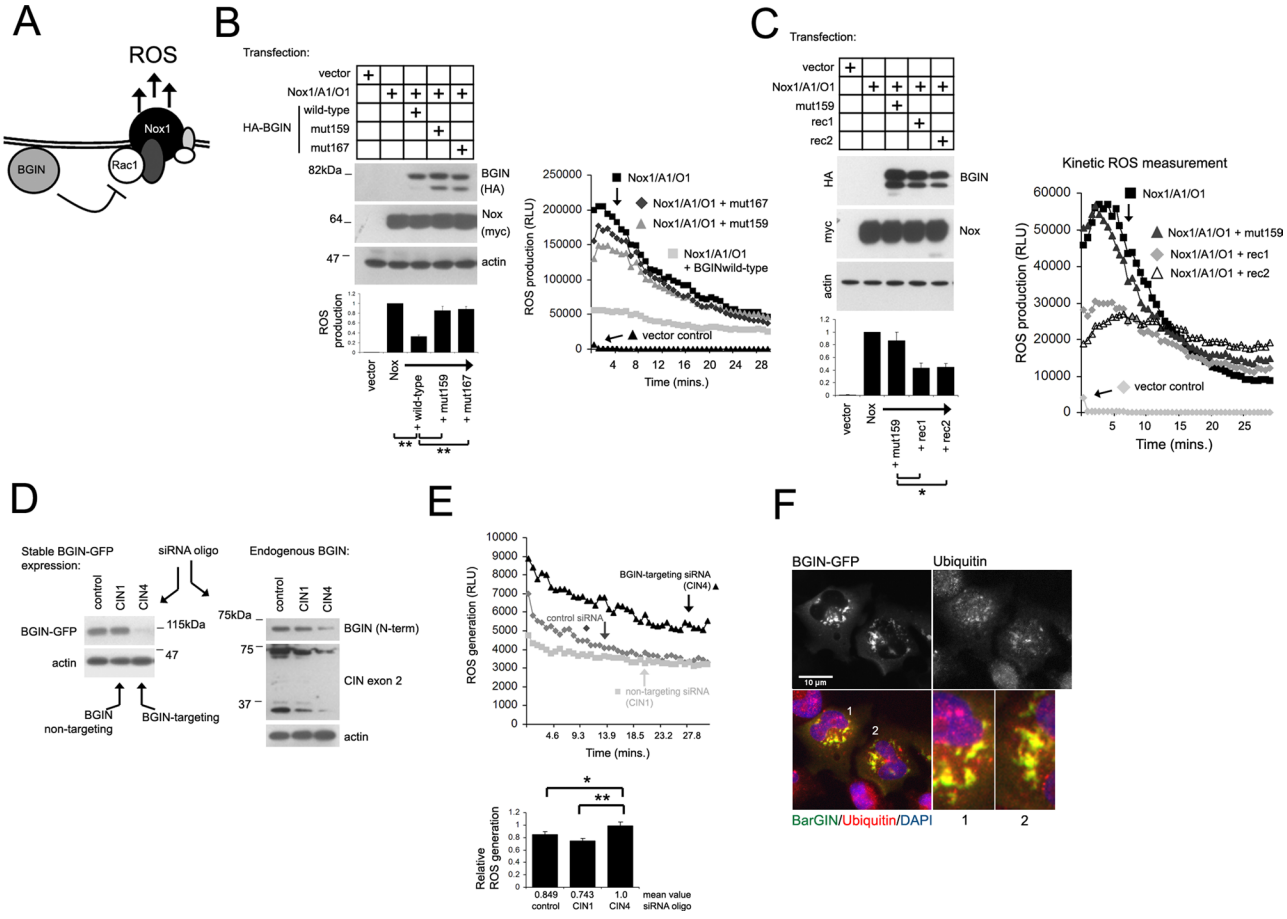

FIGURE 6: BGIN inhibits ROS generation through the membrane-associated Nox1 complex. (A) The Nox1 complex and its activator/organizer components NoxA1 and NoxO1 (and the ubiquitous p22 subunit) mediate ROS generation through Rac1. A membrane-associated BGIN population may modulate membranous Rac1 activity to attenuate Nox1-dependent ROS generation. (B) Uncoupling BGIN/poly-Ub interactions attenuates BGIN inhibition of Nox1-dependent ROS generation. NoxO1/NoxA1/Nox1 and BGIN constructs were transfected in HEK293T cells as described earlier and processed for chemiluminescence/immunoblotting. (C) Recoupling BGIN/poly-Ub interactions restores BGIN inhibition of Nox1-dependent ROS generation. HEK293T cells were transfected and processed for chemiluminescence/immunoblotting as described. For B and C, a portion of the transfected cells was assayed for ROS activity, and lysates from the remainder were probed for myc-NoxA1/O1 and BGIN expression. Quantification of ROS generation by chemiluminescence assay is shown below with transfection of all three Nox (O1/A1/Nox1) components (last lane) set to 1.0, with all other samples expressed as a comparative ratio (mean ± SE of triplicate samples). A kinetic curve measurement from a representative sample is shown in the line graph (ROS is measured in relative light units [RLU]). (D) siRNA-directed depletion of BGIN in SH-SY5Y cells. Cells transfected with 20 nM siRNAs in stably expressing BGIN SH-SY5Y (left) or normal SH-SY5Y cells (right) were immunoblotted for the components indicated. (E) BGIN depletion increases ROS generation. SH-SY5Y cells transfected with the BGIN-targeting CIN4 oligo result in a slight elevation of ROS generation. Bar graphs from B, C, and E are derived from average ± SE of mean values from at least four independent experiments (**$p < 0.002$, *$p < 0.02$) and normalized as described, with a representative kinetic ROS measurement depicted in adjacent line graphs. (F) BGIN overexpression results in colocalization with Ub at perinuclear granules. BGIN-GFP–expressing cells were costained for Ub, and BGIN-GFP perinuclear tubules were examined for Ub staining. Magnified view of perinuclear BGIN-tubule clusters are numbered in merged color images (bottom) and displayed adjacently in numbered magnified panels.

in Ub inclusions would be a pathologically terminal event that would not necessarily be informative with respect to changes in the BGIN pathway, we separately examined changes in BGIN membrane distribution in AD, PD, HD, and control brain tissue by biochemical fractionation (see Workflow outline, Supplemental Figure S7A).

Using the BGIN-specific antibody targeting the recoded BGIN N-terminus, we determined whether BGIN could accumulate in pathological Ub-enriched aggregates such as Lewy bodies, amyloid plaques, or neurofibrillary tangles in human brain. We observed increased BGIN immunoreactivity in AD-associated neurofibrillary tangles in both human brain (Figure 7A, top right) and APP transgenic mice (Figure 7A, bottom right). Approximately 20% of neurofibrillary tangles labeled with thioflavin S also showed increased BGIN immunoreactivity. Although some BGIN colocalization with Ub in tangles was evident in human AD brain (Supplemental Figure S7B), BGIN accumulation was not detected in amyloid plaques and dystrophic neurites in AD brain or Lewy bodies in dementia with Lewy bodies/PD cases (Supplemental Figure S7C). We then determined by immunohistochemical staining whether BGIN and Rac1 could both accumulate in neurofibrillary tangles. We found good

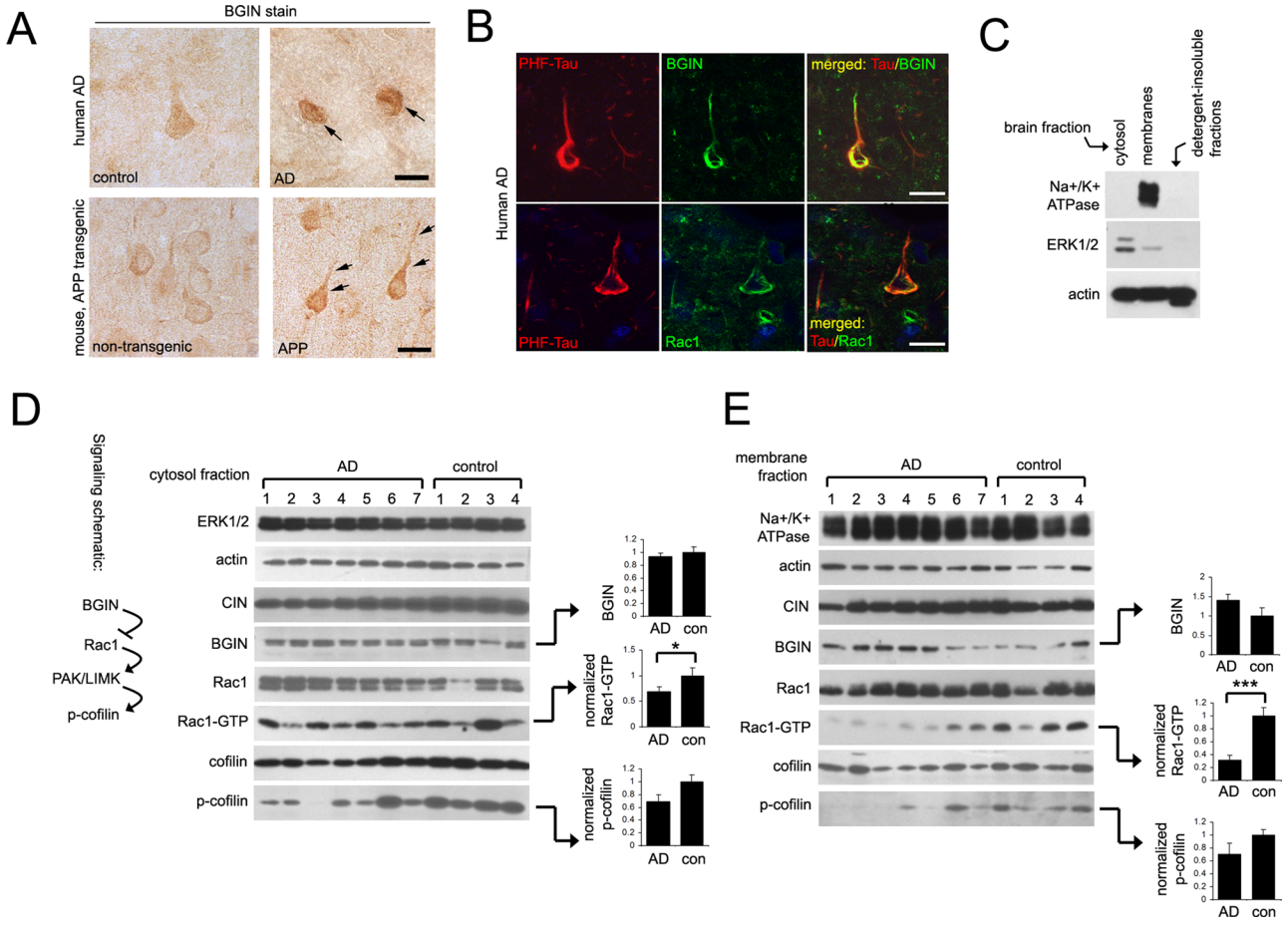

FIGURE 7: BGIN localizes to fibrillary tangles and partitions to membranes in AD. (A) BGIN is present in dense-staining pathological aggregates in AD brain. Cortical control/AD sections from human patients (top) or control/APP transgenic mice (bottom) were stained with an affinity-purified BGIN antibody recognizing the unique BGIN N-terminus (bar,10 μm). (B) BGIN and Rac1 localize to neurofibrillary tangles in AD. Human AD brain sections were stained using antibodies labeling BGIN (top) or Rac1 (bottom; green) and costained with a fluorescent antibody for pTau (PHF; red). Merged panels are displayed adjacently (bar, 10 μm). (C) Cytosolic, detergent-soluble membranes and insoluble fractions were generated from human brain tissue by ultracentrifugation as described in the Supplemental Methods. A 30-μg amount of protein from cytosol, membranes, and insoluble fractions from a control sample was immunoblotted for ERK1/2, Na^+/K^+ ATPase, and actin to determine the fractionation quality. (D) Left, signaling schematic of the BGIN/Rac1 pathway probed. Cytosolic (D) and detergent-soluble membrane fractions (E) from brain tissue of seven AD (numbered 1–7) and four control (1–4) patients were immunoblotted for the components indicated. BGIN, Rac1-GTP (normalized for total Rac1) and p-cofilin (normalized with total cofilin) bands are expressed as averages ± SE between groups, with the control mean set to 1.0 (*$p < 0.05$, ***$p < 0.002$).

colocalization of BGIN and Rac1 with pTau-staining (PHF-Tau) tangles in human AD brain (Figure 7B), indicating that pathological accumulation of BGIN and Rac1 coincides with neurofibrillary tangles. Taken together, these results indicate that Ub accumulation can also potentially influence BGIN aggregation in AD tangles.

Next we determined whether biochemical BGIN distribution and downstream signaling components were influenced in a neurodegenerative context. Surveying AD, PD, and HD tissues for differential BGIN distribution, we found that membrane-associated BGIN was elevated in AD brain (Supplemental Figure S7, D–F). We then generated biochemical membrane fractions from an expanded AD/control brain tissue cohort (Figure 7C) and determined whether BGIN abundance in cytosol/membrane compartments coincided with downstream Rac1 inactivation and consequent cofilin phosphorylation (p-cofilin) through the PAK/LIMK pathway (Figure 7D, signaling schematic). BGIN was generally found to be more abundant in AD membranes, which correlated with decreased Rac1-GTP and p-cofilin levels (Figure 7E). Little difference was seen in BGIN levels between AD and control cytosol (Figure 7D). Comparing BGIN abundance, Rac1 activity, and p-cofilin levels in individual samples within the sample cohort, we found that individuals with more membranous BGIN also demonstrated less membrane-associated Rac1 activity (Supplemental Figure S7G). Taken together, these results demonstrate a tight correlation between membrane BGIN distribution and downstream Rac1 activation, suggesting that BGIN signaling may be altered in AD proteotoxicity.

Determining a role for BGIN in Rac1 inactivation with APP proteotoxicity

So far, our results suggest that proteotoxicity in AD may influence BGIN signaling and downstream Rac1 function. To further investigate whether BGIN may directly play a role in modulating Rac1

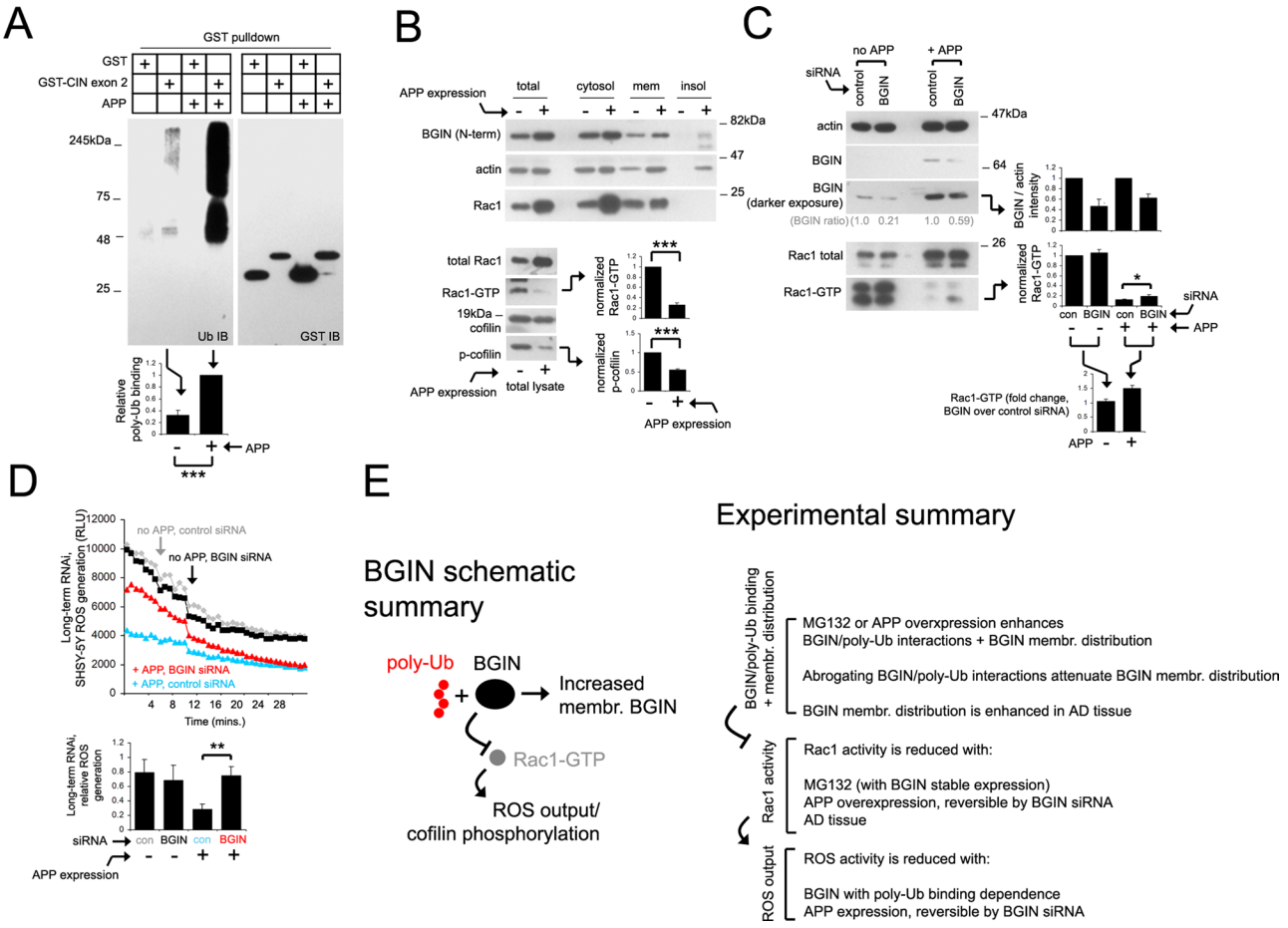

FIGURE 8: Determining a role for BGIN in Rac1 signaling with APP proteotoxicity. (A) Probing poly-Ub/CIN exon 2 interactions in APP-expressing SH-SY5Y cells. GST or GST-CIN exon 2 was expressed and precipitated from untransfected or APP-expressing SH-SY5Y cells as indicated and immunoblotted for GST or Ub. Graph indicates poly-Ub smear band density normalized to GST-CIN exon 2 precipitates from three experiments. (B) Stable APP expression attenuates Rac1 activity. Top, normal or APP-expressing SYSH5Y cells were processed to generate total, cytosolic, membrane, or insoluble fractions and immunoblotted. Bottom, total lysates were assayed for Rac1 activity by PBD pull-down assay or cofilin phosphorylation with or without APP expression. (C) Long-term BGIN siRNA treatment elevates Rac1-GTP levels in APP-expressing cells. Normal or APP-expressing SH-SY5Y cells were transfected for three rounds of siRNA as described in the Supplemental Methods and subjected to Rac1-GTP analysis by PBD pull-down assay. Fold change in Rac1-GTP levels with long-term BGIN siRNA treatment in comparison to controls (set to 1.0) were calculated in the lower bar graphs. (D) Cells were transfected as described in C and subjected to chemiluminescence assay for ROS output. Kinetic ROS output values are shown in the upper line graph, and relative ROS values from three experiments measured in triplicate are depicted in the lower bar graph. All bar graph values (B–D) represent mean ± SE from a minimum of three experiments (**$p < 0.01$, ***$p < 0.002$). Paired *t* test values were tabulated for C (*$p < 0.02$). (E) Left, schematic summary of poly-Ub/BGIN interactions and consequent effects on Rac1/ROS generation. Right, experimental summary of results supporting the key features of the model.

activity in AD, we used a transgenic SH-SY5Y cell model stably expressing APP (Kounnas *et al.*, 2010). Stable APP expression resulted in a 50-fold increase in $A\beta_{1-42}$ production (Supplemental Figure S8A), confirming the overproduction of proteotoxic Aβ species in these cells. We observed a dramatic enhancement in CIN exon 2/poly-Ub and full-length BGIN/poly-Ub interactions in the APP-expressing cell line compared with nonexpressing cells (Figure 8A and Supplemental Figure S8B). We also found a slight increase in membrane-associated BGIN and a dramatic reduction in Rac1 activation and cofilin phosphorylation with APP expression (Figure 8B). Of interest, attenuated Rac1 activity correlated with attenuated ROS generation with APP proteotoxicity (Supplemental Figure S8C).

We next determined whether BGIN depletion could modulate Rac1 activity in normal or transgenic APP contexts. We found that short-term BGIN small interfering RNA (siRNA) transfection (48 h) had little effect on Rac1 activity in wild-type or APP-expressing SH-SY5Y cell lines (Supplemental Figure S8, D and E), which was accompanied by little or no change in ROS output in APP cells with BGIN transfection (Supplemental Figure S8F). However, we found that long-term BGIN siRNA treatment (continuous siRNA transfection over 4–6 d; see the Supplemental Methods) produced a 50% increase in Rac1 activity in an APP-transgenic background, with little change in SH-SY5Y cells (Figure 8C and Supplemental Figure S8G). Of interest, we find that Rac1-GTP levels with BGIN siRNA treatment are not restored to levels observed with wild-type cells, possibly because BGIN depletion was consistently partial. However, the possibility remains that other Rac1 regulators aside from BGIN might be involved in inactivating Rac1 with APP overexpression.

We then determined whether long-term BGIN siRNA treatment also affected ROS output in SH-SY5Y cells. In agreement with the Rac1-GTP profile observed, APP cells also demonstrated a concomitant increase in ROS output with long-term BGIN siRNA treatment (Figure 8D). This indicates that Rac1 regulatory components may normally compensate for short-term depletion of BGIN levels, and prolonged BGIN depletion can elevate Rac1 activity and downstream ROS generation in response to APP proteotoxicity.

Taken together, these results suggest that chronic APP overexpression down-regulates Rac1 activity and downstream ROS generation. Furthermore, BGIN contributes to Rac1 deactivation and ROS output with APP overexpression, as BGIN depletion can partially reverse both Rac1 and ROS generation in an APP proteotoxic context. These results contribute additional evidence that poly-Ub/BGIN interactions may contribute to downstream Rac1 signaling with neurodegenerative proteotoxicity (Figure 8E).

DISCUSSION

BGIN is a unique member of the BAR-RhoGAP family of adaptors generated by combining exons from neighboring 3BP1 and CIN gene loci. This represents a novel alternative splicing mechanism ultimately appending unique BGIN sequence modules at both N- and C-terminal ends. Recoding of the BGIN N-terminus through exon 2 excision and consequent CTG initiation results in a unique 42-aa stretch. Although translation using noncanonical Met residues is not common, instances where CTG initiation codons are used have been described to include thioredoxin/glutathione reductase and FGF2 (Arnaud *et al.*, 1999; Gerashchenko *et al.*, 2010). Deletion of this 42-aa stretch is inconsequential to dimerization of the BAR domain (Huang, Bokoch, and DerMardirossian, unpublished results) and leaves the functional role of this unique sequence a subject for future study.

BGIN can also be distinguished from other BAR-RhoGAP components through the exchange of the prototypical polyproline-rich repeat region for a unique C-terminal poly-Ub–binding domain. Multiple ubiquitin-binding modules have been characterized in higher eukaryotes, including the ubiquitin-interacting motif and CUE, UBA, UBAN, UEV, GAT, NZF, and GLUE domains, among many others (Dikic *et al.*, 2009). These Ub-coupling domains bind Ub-conjugated components at membrane platforms to facilitate their sorting to endosomes and multivesicular bodies. We describe here a novel poly-Ub–binding domain, the CIN exon 2 module, which exhibits specificity for poly-Ub chains and mediates the distribution of BGIN to membranes to limit membrane-associated Rac1 activity (Figure 8E). Although we cannot exclude the possibility that BGIN may also localize to endomembrane compartments at this point, Rac1 function at the plasma membrane compartment has been well established, and our results using the Nox1 effector system support the notion that at BGIN distributes to the plasma membrane to some extent. This represents a unique membrane-shuttling mechanism for BAR-domain components, as BAR domains commonly dock to membrane platforms with the aid of classic lipid-binding modules such as PX and PH domains (Rao and Haucke, 2011).

Neuronal Ub aggregates are a hallmark of neurodegenerative disease and distinctively appear in Lewy body inclusions in PD, nuclear inclusions in HD, and neurofibrillary tangles in AD (Alves-Rodrigues *et al.*, 1998). Proteasomal dysfunction and accumulation of poly-Ub conjugates in neurofibrillary tangles are related phenomena previously described in AD (Mori *et al.*, 1987; Keller *et al.*, 2000). Downregulation of Rac1 activity was also previously implicated in AD, as downstream Rac1 effectors such as the PAKs exhibit attenuated activity and altered distribution in human AD and transgenic APP murine models (Zhao *et al.*, 2006; Ma *et al.*, 2008). However, how upstream regulators attenuate Rac1 activity in response to neurodegenerative stress and proteotoxicity remains elusive. Our results suggest that BGIN operates as part of a redundant system of Rac1 regulators, and its depletion may not influence total Rac1 activity under steady-state conditions. However, BGIN activity might be more influential to Rac1-GTP in the context of proteotoxic stimuli, as Rac1 activity and effector function are influenced by BGIN depletion with APP overexpression.

Our results also indicate that BGIN overexpression in tissue culture cells produces Ub-enriched BGIN aggregates in a manner dependent on its C-terminal poly-Ub interaction domain, suggesting that pathophysiological Ub accumulation and aggregation might also influence BGIN accumulation in certain neurodegenerative settings. Although BGIN accumulation was observed in AD neurofibrillary tangles, we were surprised to find no enrichment of BGIN in Ub-enriched Lewy bodies (Alves-Rodrigues *et al.*, 1998). This might suggest that compositional differences or other mechanistic factors might be involved in excluding BGIN from PD aggregates or in specifically recruiting BGIN into AD tangles. Because proteasomal dysfunction and Ub aggregation is also found in other neurodegenerative disorders such as Pick's disease, amyotrophic lateral sclerosis, progressive supranuclear palsy, and Machado–Joseph disease (Alves-Rodrigues *et al.*, 1998), we anticipate future studies to investigate potential BGIN/Ub interaction in other neurodegenerative proteotoxicity models.

BGIN membrane distribution in response to proteasomal stress or in AD tissue potentially affects numerous Rac1 effector pathways, such as the modulation of membrane-associated ROS generation through the NOX complex. Rac-responsive NOX complexes such as Nox1 and 2 are present in neurons, astrocytes, and microglia (Sorce and Krause, 2009), and recent evidence indicates that Nox1 and Nox3 expression is upregulated in brain early in AD (de la Monte and Wands, 2006). ROS generation through Nox2 contributes to physiological and behavioral defects associated in AD, as Nox2 deletion reversed behavioral and pathological deficits in APP transgenic mice models (Park *et al.*, 2008). Thus a system such as BGIN to limit Rac-dependent NOX activity might be beneficial to delay ROS-induced neurophysiological decline and attenuate cytotoxicity in AD.

Rac1 has been recently shown to be polyubiquitylated by E3 ubiquitin ligases such as XIAP, c-IAP, and HACE1 (Torrino *et al.*, 2011; Oberoi *et al.*, 2012). Polyubiquitylation by these E3 ligases is enhanced by Rac1 activation, thereby presenting a unique homeostatic mechanism for limiting Rac1 activity. Interaction between the BGIN CIN exon 2 domain and poly-Ub presents an intriguing scenario in which Rac1 polyubiquitylation may enhance BGIN/Rac1 interactions, thereby promoting Rac1 inactivation. Our observation that Rac1 and BGIN can reside together in neurofibrillary tangles also leaves us to ask whether polyubiquitylated Rac1 might be the primary Rac1 species in these ubiquitin aggregates. Because the spatial regulation of Rac1 is critical to the activation of Rac1 effector pathways, we anticipate that potential interactions between BGIN and polyubiquitylated Rac1 might contribute an additional means to down-regulate Rac1 activity within a compartmentalized region.

In summary, we have described a novel role for a brain-specific BAR-RhoGAP splice variant, BGIN, in binding poly-Ub, which mediates its distribution to membrane compartments. Inactivation of Rac1 by BGIN in response to MG132 in cultured cells and in an APP-overexpression model of AD suggests that BGIN might relay proteotoxic signals through pathological poly-Ub accumulation. BGIN membrane docking through poly-Ub interactions might also serve

as a prototypical model of how protein–protein interactions could shuttle BAR-RhoGAP family members to membrane compartments and contributes to our understanding of how RhoGTPase signals are spatially separated.

MATERIALS AND METHODS

Cell culture and transfection

HeLa, HEK293T, SH-SY5Y, and Neuro 2A cells were cultured in DMEM supplemented with 8% fetal bovine serum. SH-SY5Y cells stably expressing APP_{751} were generously provided by S. Wagner (University of California, San Diego; Kounnas *et al*., 2010) and cultured in media containing 500 μg/ml Geneticin. Lipofectamine Plus reagent (Invitrogen, Carlsbad, CA) was used for transient transfection of all cells as described according to specifications from the manufacturer. Lipofectamine 2000 was used for transfection of siRNA oligonucleotides as previously described (Huang *et al*., 2008) in HeLa cells. siRNA transfection conditions for SH-SY5Y cells are described later and in the Supplemental Methods.

Plasmid constructs and antibodies

All constructs used in this study are described in the Supplemental Methods. Antibodies for immunoblotting include the 23A8 monoclonal antibody for Rac1 (Millipore, Billerica, MA), epidermal growth factor receptor, GST, and P4D1 monoclonal anti-Ub (Santa Cruz Biotechnology, Santa Cruz, CA), Na^+/K^+ ATPase (Millipore), actin (MP Biomedicals, Solon OH), 9E10 monoclonal antibody to detect the myc epitope, 12CA5 antibody to detect hemagglutinin (HA), GFP (Invitrogen), and ERK1/2 (Cell Signaling, Danvers MA). ERGIC, giantin, and protein disulfide isomerase (PDI) antibodies were kindly provided by William Balch and Sandra Schmid (Scripps Research Institute).

Protein purification

Purification of all BGIN proteins subjected to proteomic analysis by mass spectrometry is described in the Supplemental Methods.

RNA interference

HeLa cells were transfected with CIN-specific synthetic siRNA oligo duplex (Dharmacon, Lafayette, CO) sequences 5′-GCGCCGUGCUUGUGGGCUA-3′ (CIN1, BGIN nontargeting) and 5′-GCACGCUUAUGGUGGGUGA-3′ (CIN4, BGIN targeting) at a final concentration of 10 nM using Lipofectamine 2000. Control siRNA oligos comprised a nontargeting siRNA pool (Dharmacon D-001206-13-20; Gohla *et al*., 2005) transfected at identical concentrations and conditions. Cells were processed for biochemical analysis 48 h after transfection.

SH-SY5Y cells were transfected with the control (nontargeting) siRNA oligonucleotide sequence 5′-GCGCGCUAUGUAGGAUUCG-3′, CIN1, or CIN4 oligos as described at a final concentration of 20 nM using RNAiMAX transfection reagent (Invitrogen). Detailed transfection conditions can be found in the Supplemental Methods.

Statistical analyses

All statistical analyses presented were calculated using two-tailed Student's *t* tests where $p < 0.05$ indicates statistical significance.

ACKNOWLEDGMENTS

We dedicate this article to the memory of Gary M. Bokoch. Special thanks go to Eric Jan, Vincent Mauro, Ganghui Liu, Ya-Wen Liu, and members of the DerMardirossian/Bokoch lab for helpful input and suggestions and to Yun-Cai Liu (La Jolla Institute for Allergy and Immunology, La Jolla, CA), Ivan Dikic (Goethe University, Frankfurt, Germany), David Komander (Medical Research Council, Cambridge, United Kingdom), and Steven Wagner (University of California, San Diego) for reagents used in this study. This work was supported by National Institutes of Health grants to G.M.B. and C.D.M. (GM044428) and to E.M. (AG5131 and AG18440). T.X., A.S., J.J.M., and J.R.Y. were supported by the National Center for Research Resources (5P41RR011823-17), the National Institute of General Medical Sciences (8 P41 GM103533-17), and the National Institute on Aging (R01AG027463-04). T.Y.H. was supported in part by a postdoctoral fellowship from the American Heart Association, Western Affiliate (0725230Y).

REFERENCES

Alves-Rodrigues A, Gregori L, Figueiredo-Pereira ME (1998). Ubiquitin, cellular inclusions and their role in neurodegeneration. Trends Neurosci 21, 516–520.

Arnaud E, Touriol C, Boutonnet C, Gensac MC, Vagner S, Prats H, Prats AC (1999). A new 34-kilodalton isoform of human fibroblast growth factor 2 is cap dependently synthesized by using a non-AUG start codon and behaves as a survival factor. Mol Cell Biol 19, 505–514.

Bedard K, Krause KH (2007). The NOX family of ROS-generating NADPH oxidases: physiology and pathophysiology. Physiol Rev 87, 245–313.

Benard V, Bohl BP, Bokoch GM (1999). Characterization of rac and cdc42 activation in chemoattractant-stimulated human neutrophils using a novel assay for active GTPases. J Biol Chem 274, 13198–13204.

Billuart P *et al*. (1998). Oligophrenin-1 encodes a rhoGAP protein involved in X-linked mental retardation. Nature 392, 923–926.

Bokoch GM (2003). Biology of the p21-activated kinases. Annu Rev Biochem 72, 743–781.

Cicchetti P, Mayer BJ, Thiel G, Baltimore D (1992). Identification of a protein that binds to the SH3 region of Abl and is similar to Bcr and GAP-rho. Science 257, 803–806.

Cicchetti P, Ridley AJ, Zheng Y, Cerione RA, Baltimore D (1995). 3BP-1, an SH3 domain binding protein, has GAP activity for Rac and inhibits growth factor-induced membrane ruffling in fibroblasts. EMBO J 14, 3127–3135.

de la Monte SM, Wands JR (2006). Molecular indices of oxidative stress and mitochondrial dysfunction occur early and often progress with severity of Alzheimer's disease. J Alzheimers Dis 9, 167–181.

Dikic I, Wakatsuki S, Walters KJ (2009). Ubiquitin-binding domains—from structures to functions. Nat Rev Mol Cell Biol 10, 659–671.

Fonda ML (1992). Purification and characterization of vitamin B6-phosphate phosphatase from human erythrocytes. J Biol Chem 267, 15978–15983.

Gerashchenko MV, Su D, Gladyshev VN (2010). CUG start codon generates thioredoxin/glutathione reductase isoforms in mouse testes. J Biol Chem 285, 4595–4602.

Gohla A, Birkenfeld J, Bokoch GM (2005). Chronophin, a novel HAD-type serine protein phosphatase, regulates cofilin-dependent actin dynamics. Nat Cell Biol 7, 21–29.

Huang TY, Minamide LS, Bamburg JR, Bokoch GM (2008). Chronophin mediates an ATP-sensing mechanism for cofilin dephosphorylation and neuronal cofilin-actin rod formation. Dev Cell 15, 691–703.

Jaffe AB, Hall A (2005). Rho GTPases: biochemistry and biology. Annu Rev Cell Dev Biol 21, 247–269.

Keller JN, Hanni KB, Markesbery WR (2000). Impaired proteasome function in Alzheimer's disease. J Neurochem 75, 436–439.

Knaus UG, Heyworth PG, Evans T, Curnutte JT, Bokoch GM (1991). Regulation of phagocyte oxygen radical production by the GTP-binding protein Rac 2. Science 254, 1512–1515.

Komander D, Reyes-Turcu F, Licchesi JD, Odenwaelder P, Wilkinson KD, Barford D (2009). Molecular discrimination of structurally equivalent Lys 63-linked and linear polyubiquitin chains. EMBO Rep 10, 466–473.

Kounnas MZ *et al*. (2010). Modulation of gamma-secretase reduces beta-amyloid deposition in a transgenic mouse model of Alzheimer's disease. Neuron 67, 769–780.

Ma QL, Yang F, Calon F, Ubeda OJ, Hansen JE, Weisbart RH, Beech W, Frautschy SA, Cole GM (2008). p21-activated kinase-aberrant activation and translocation in Alzheimer disease pathogenesis. J Biol Chem 283, 14132–14143.

Mori H, Kondo J, Ihara Y (1987). Ubiquitin is a component of paired helical filaments in Alzheimer's disease. Science 235, 1641–1644.

Nakano-Kobayashi A, Kasri NN, Newey SE, Van Aelst L (2009). The Rho-linked mental retardation protein OPHN1 controls synaptic vesicle endocytosis via endophilin A1. Curr Biol 19, 1133–1139.
Oberoi TK *et al.* (2012). IAPs regulate the plasticity of cell migration by directly targeting Rac1 for degradation. EMBO J 31, 14–28.
Park L *et al*. (2008). Nox2-derived radicals contribute to neurovascular and behavioral dysfunction in mice overexpressing the amyloid precursor protein. Proc Natl Acad Sci USA 105, 1347–1352.
Parrini MC *et al.* (2011). SH3BP1, an exocyst-associated RhoGAP, inactivates Rac1 at the front to drive cell motility. Mol Cell 42, 650–661.
Price LS, Leng J, Schwartz MA, Bokoch GM (1998). Activation of Rac and Cdc42 by integrins mediates cell spreading. Mol Biol Cell 9, 1863–1871.
Rao Y, Haucke V (2011). Membrane shaping by the Bin/amphiphysin/Rvs (BAR) domain protein superfamily. Cell Mol Life Sci 68, 3983–3993.
Richnau N, Aspenstrom P (2001). Rich, a rho GTPase-activating protein domain-containing protein involved in signaling by Cdc42 and Rac1. J Biol Chem 276, 35060–35070.
Sorce S, Krause KH (2009). NOX enzymes in the central nervous system: from signaling to disease. Antiox Redox Signal 11, 2481–2504.
Stofega M, DerMardirossian C, Bokoch GM (2006). Affinity-based assay of Rho guanosine triphosphatase activation. Methods Mol Biol 332, 269–279.
Tcherkezian J, Lamarche-Vane N (2007). Current knowledge of the large RhoGAP family of proteins. Biol Cell 99, 67–86.
Torrino S, Visvikis O, Doye A, Boyer L, Stefani C, Munro P, Bertoglio J, Gacon G, Mettouchi A, Lemichez E (2011). The E3 ubiquitin-ligase HACE1 catalyzes the ubiquitylation of active Rac1. Dev Cell 21, 959–965.
Zhao L *et al.* (2006). Role of p21-activated kinase pathway defects in the cognitive deficits of Alzheimer disease. Nat Neurosci 9, 234–242.